Stability Analysis of a Multi-Machine Parallel Microgrid Using a Time-Domain Method

Boning Chang and Yifeng Ren *

Posted Date: 23 October 2025

doi: 10.20944/preprints202510.1718.v1

Keywords: multi-node system; stability analysis; microgrid; time-domain analysis

 doi:10.20944/preprints202510.1718.v1

Article

Stability Analysis of a Multi-Machine Parallel Microgrid Using a Time-Domain Method

Boning Chang and Yifeng Ren *

North University of China, Taiyuan 030051, China

* Correspondence: renyifeng126@126.com

Abstract

Current microgrid research primarily focuses on radial topologies and their control strategies, while exploration of the time-domain dynamic behavior of closed-loop controlled microgrids remains relatively insufficient. This research gap makes it difficult to directly observe and deeply analyze the evolution mechanisms of critical phenomena， such as oscillations and instability, when they occur. Therefore, conducting time-domain analysis on closed-loop structures is crucial for revealing system instability mechanisms and ensuring their safe and stable operation. This paper establishes a state-space model for a closed-loop microgrid structure composed of multiple parallel inverters and conducts time-domain stability analysis under grid-connected operation. First, a mathematical model of the closed-loop microgrid system is constructed using state-space equations. Subsequently, time-domain analysis of small-signal stability is performed on the model. By varying key parameters such as the droop coefficient, the influence patterns on system stability are investigated. The results indicate that the droop control coefficient and LC filter parameters exert the most significant impact on system dynamic characteristics. Simulation experiments validate the correctness and effectiveness of the theoretical model. Finally, the time-domain characteristics of this model were further analyzed and validated through simulations. Results demonstrate that the system maintains robust stability under disturbances even in grid-connected mode.

Keywords: multi-node system; stability analysis; microgrid; time-domain analysis

1. Introduction

In recent years, the problem of environmental pollution caused by traditional fossil fuels has become more and more serious, and has become a major issue in today's world economic development. Renewable energy based on wind energy and solar energy provides an effective solution to the current problems [1,2]. The combination of the innovation of small distributed generation systems and the technological advancement of power electronic systems has given rise to the concept of future network technologies, such as microgrids. With the advancement of global energy transformation and the 'dual carbon' goal, microgrids have become an important part of the new power system due to their flexibility, low-carbon nature, and reliability. Many forms of distributed generation, such as fuel cells, photovoltaic power generation, and micro turbines, are connected to the grid through power electronic converters [3]. The microgrid can operate in grid-connected mode or stand-alone mode. However, the uncertainty of renewable energy generation has brought a series of problems to the safe and stable operation of microgrid [4,5]. There are a large number of power electronic converters in the microgrid. The increase of various micro-sources will significantly affect the characteristics of the microgrid, and the microgrid exhibits nonlinear characteristics such as low inertia, low damping, and strong time-variability. These problems make the system more prone to oscillation instability [6,7]. Even if each sub-unit is stable on its own, the interaction between the sub-units will cause stability problems in the system [8]. Therefore, it is necessary to model and analyze the stability of the microgrid.

 doi:10.20944/preprints202510.1718.v1

In the research of microgrid, how to ensure the power quality and system stability in both grid-connected and islanded operation modes has always been one of the key technical challenges. Whether operating in parallel with the main network or independently, there will be some possible problems that can lead to system instability.

In power system networks, voltage and frequency are the two most critical operational parameters [9]. One of the most fundamental and valuable operational modes of a microgrid is islanded operation. In this mode, the microgrid disconnects from the main grid (macrogrid) and operates independently, relying entirely on its internal distributed energy resources—such as photovoltaics, wind turbines, battery energy storage systems, and diesel generators—to provide continuous and reliable power to a local area. [10,11]. When the system is unstable, it is often difficult for the system to maintain the stability of voltage and frequency independently [12–14]. Compared with radial microgrids, closed-loop microgrids can significantly mitigate these issues. In the event of a line fault, power can be supplied from the opposite end through the closed-loop path without interrupting critical loads. Furthermore, when a grid-forming control strategy is adopted, the stability and operational reliability of the microgrid can be substantially enhanced.

Grid-Forming Control (GFM) is an advanced control strategy for power electronic converters that enables them to emulate the operational behavior of traditional synchronous generators, thereby autonomously establishing and maintaining grid voltage and frequency. Droop control is one of the most widely used methods in grid-connected inverter control. It emulates the active power-frequency (P–f) and reactive power-voltage (Q–V) droop characteristics of synchronous generators. In power systems with a high penetration of renewable energy, grid-forming inverters—which operate without relying on grid synchronization signals—can autonomously regulate the voltage and frequency. This capability significantly enhances the system stability and resilience to disturbances, and helps mitigate stability challenges resulting from weakened grid strength [15–17].

The application in a weak grid environment poses a unique challenge to the stability of grid-connected inverters. A weak grid has the characteristics of low short-circuit capacity and low inertia. Therefore, it is necessary to explore strategies to improve the stability and performance of inverters in this challenging environment [18,19]. In [20], it estimates the interaction and stability of grid-connected inverters equipped with LC filters. The resonance and oscillation characteristics of multiple inverters are analyzed through simulation. An interactive admittance model is proposed to effectively characterize these interactions in relation to the physical network admittance. Frequency-domain stability analysis of the microgrid model enables early prediction of oscillatory instability and facilitates stability assessment at specific frequency points. However, this paper does not examine time-domain characteristics; as a result, the impact of specific parameters on system stability remains unclear. In practical applications, system stability may be vulnerable to variations in these parameters. In [21], a comprehensive dynamic model of the network is established, with each module represented in state-space form and integrated into the overall system. Sensitivity analysis is conducted on the full network model to evaluate the influence of key parameters on system stability. However, this study is restricted to the dynamic model of a radial network, which is prone to instability in the event of sudden circuit breakages. Although closed-loop networks provide higher power supply reliability and improved stability, they also introduce greater operational and analytical complexity. In [22], a steady-state analysis is carried out for a microgrid system consisting of multiple inverters operating under droop control, and a state-space model is developed to examine the impact of droop coefficients on system stability. The study focuses exclusively on radial microgrid configurations and does not investigate closed-loop microgrids under droop control. Although employing multiple droop-controlled inverters in a closed-loop microgrid can enhance operational stability in practice, it also increases structural and control complexity.

Under the current research framework, this paper focuses on the structural modeling of microgrids. For a closed-loop microgrid system composed of multiple parallel inverters, a state-space model is developed using time-domain analysis. Then, eigenvalue analysis and parameter sensitivity analysis are conducted. Based on the theoretical findings, a corresponding simulation model is built

 doi:10.20944/preprints202510.1718.v1

in the MATLAB/Simulink R2024a environment, and experimental results validate the accuracy and effectiveness of the theoretical model in characterizing the dynamic behavior of the system. Finally, the influence of parameter variations on system stability is summarized, providing theoretical guidance for parameter design in practical engineering applications.

Based on the current research, this paper focuses on modeling microgrid structures. For a closed-loop microgrid system comprising multiple parallel inverters, a mathematical model based on the state-space method has been established. Through eigenvalue analysis and parameter sensitivity analysis, an in-depth investigation of system stability was conducted, alongside time-domain dynamic response analysis under grid-connected operation. Based on theoretical findings, a corresponding simulation model was constructed within the MATLAB/Simulink R2024a platform. Experimental results demonstrate that the theoretical model accurately and effectively characterizes the system's dynamic behavior. The study summarises the influence patterns of parameter variations on system stability and reveals the dynamic performance of the system under grid-connected operation when minor disturbances are present. It further demonstrates that the investigated system possesses disturbance rejection capabilities to handle small load variations during routine operation. This validates the rationality and feasibility of the system design from a dynamic performance perspective, laying a solid foundation for its practical application and promotion in engineering practice.

2. Materials and Methods

2.1. Model of Microgrid

Presently, most distributed power sources with power electronic interfaces for renewable energy generation employ three-phase inverters. Therefore, this paper focuses on a microgrid system based on three-phase inverter technology [23,24], as illustrated in Figure 1.

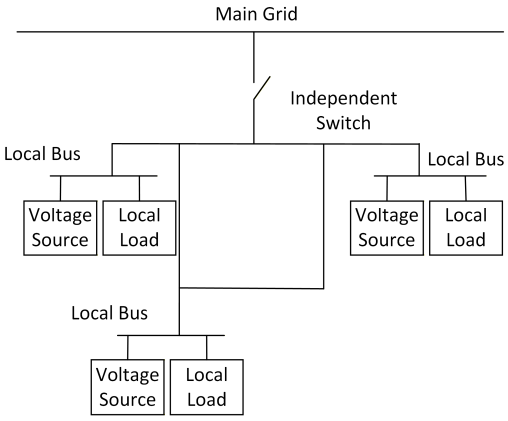

Figure 1. Schematic diagram of micro-grid structure based on the inverter.

The modeling method proposed in this paper divides the whole system into three sub-modules: inverter, network, and load. Each inverter is modeled in its own reference frame, and the rotation frequency of the microgrid system is determined by the rotation frequency of one of the selected inverters. The inverter model includes a droop power controller model, output filter model, LC filter model, and voltage and current controller model. The modules shown in Figure 2 will be explained in the following sections [25].

 doi:10.20944/preprints202510.1718.v1

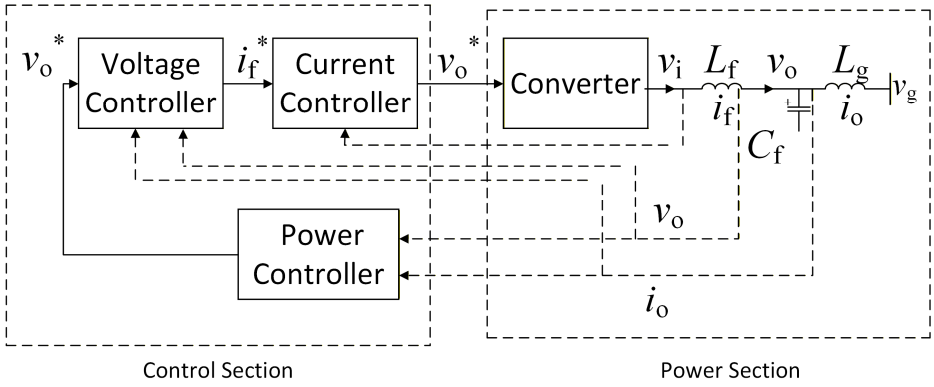

Figure 2. Control block diagram of droop control inverter.

The basic idea of droop control is to simulate the working characteristics of synchronous generators: by reducing the frequency of the output voltage to meet the increase of active power in the load, and by reducing the amplitude of the output voltage to meet the increase of reactive power in the load, the power control loop diagram is shown in Figure 3.

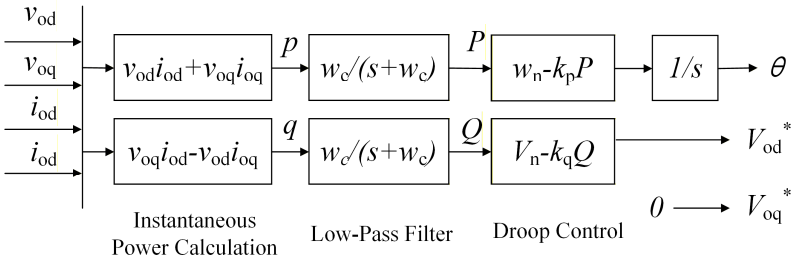

Figure 3. Power control loop diagram.

2.1.1. Modeling of a Single Inverter

By integrating the state models of each part, the overall small signal model of the droop control inverter can be obtained as follows.

$$[\Delta \dot{x}_{inv}] = A_{inv}[\Delta x_{inv}] + B_{inv}[\Delta v_{gdq}] + B_{\omega com}[\Delta \omega_{com}] \tag{1}$$

$$\begin{bmatrix} \Delta\omega \\ \Delta i_{odq} \end{bmatrix} = \begin{bmatrix} C_{inv\omega} \\ C_{invc} \end{bmatrix} [\Delta x_{inv}] \tag{2}$$

where

$$x_{inv} = \begin{bmatrix} \delta & P & Q & \varphi_{dq} & \gamma_{dq} & i_{fdq} & v_{odq} & i_{odq} \end{bmatrix}^T \tag{3}$$

$$A_{inv} = \begin{bmatrix} A_p & 0 & 0 & B_p \\ B_{v1}C_{pv} & 0 & 0 & B_{v2} \\ B_{c1}C_{pv}D_{v1} & B_{c1}C_v & 0 & B_{c1}D_{v2} + B_{c2} \\ B_{LCL1}C_{pv}D_{v1}D_{c1} & B_{LCL1}D_{c1}C_v & B_{LCL1}C_v & A_{LCL} + B_{LCL1}(D_{c1}D_{v2} + D_{c2}) \end{bmatrix} \tag{4}$$

 doi:10.20944/preprints202510.1718.v1

$$B_{inv}=\begin{bmatrix}0\\0\\0\\B_{LCL2}\end{bmatrix},B_{\omega com}=\begin{bmatrix}B_{P\omega com}\\0\\0\\0\end{bmatrix} \tag{5}$$

$$C_{inv\omega}=\begin{bmatrix}C_{P\omega} & 0 & 0 & 0\end{bmatrix} \tag{6}$$

$$C_{invc}=\begin{bmatrix}0 & 0 & 0 & \begin{bmatrix}0 & 0 & I\end{bmatrix}\end{bmatrix} \tag{7}$$

To connect the inverter to the whole system, the output variables need to be converted to the common reference frame. In this case, the output variable of the inverter is expressed as the output current of the vector, and the small signal output current on the common reference frame can be obtained by using the transformation formula, such as Park.

$$\left[\Delta i_{oDQ}\right]=\left[T_S\right]\left[\Delta i_{odq}\right]+\left[T_C\right]\left[\Delta\delta\right] \tag{8}$$

$$\left[T_S\right]=\begin{bmatrix}\cos(\delta_0) & -\sin(\delta_0)\\ \sin(\delta_0) & \cos(\delta_0)\end{bmatrix} \tag{9}$$

$$T_C=\begin{bmatrix}-I_{od}\sin(\delta_0)-I_{oq}\cos(\delta_0)\\ I_{od}\cos(\delta_0)-I_{oq}\sin(\delta_0)\end{bmatrix} \tag{10}$$

Similarly, the input signal of the inverter model is the bus voltage represented on the common reference frame. The bus voltage can be converted into a separate inverter reference frame using inverse transformation, which is given by the following formula :

$$\left[\Delta v_{gdq}\right]=\left[T_S^{-1}\right]\left[\Delta v_{gDQ}\right]+\left[T_v^{-1}\right]\left[\Delta\delta\right] \tag{11}$$

$$\left[Tv{-}1\right]=\begin{bmatrix}-V_{gD}\sin(\delta_0)+V_{gQ}\cos(\delta_0)\\ -V_{gD}\cos(\delta_0)-V_{gQ}\sin(\delta_0)\end{bmatrix} \tag{12}$$

Each independent inverter model has 13 states, 3 inputs, and 2 outputs (except for the inverter with a common reference frame, which has 3 outputs).

$$\left[\Delta\dot{x}_{inv}\right]=A_{invi}\left[\Delta x_{inv}\right]+B_{invi}\left[\Delta v_{gDQ}\right]+B_{i\omega com}\left[\Delta\omega_{com}\right]$$

$$\begin{bmatrix}\Delta\omega i\\ \Delta i_{oDQi}\end{bmatrix}=\begin{bmatrix}C_{inv\omega i}\\ C_{invci}\end{bmatrix}\left[\Delta x_{inv}\right] \tag{13}$$

$$A_{inv}=\begin{bmatrix}A_{pi} & 0 & 0 & B_{pi}\\ B_{v1i}C_{pvi} & 0 & 0 & B_{v2i}\\ B_{c1i}C_{pv}iD_{v1i} & B_{c1i}C_{vi} & 0 & B_{c1i}D_{v2i}+B_{c2i}\\ B_{LCL1i}C_{pvi}D_{v1i}D_{c1i}+B_{LCL2i}B_x & B_{LCL1i}D_{c1i}C_{vi} & B_{LCL1i}C_{vi} & A_{LCLi}+B_{LCL1i}\left(D_{c1i}D_{v2i}+D_{c2i}\right)\end{bmatrix} \tag{14}$$

$$C_{inv\omega i}=\begin{bmatrix}C_{P\omega} & 0 & 0 & 0\end{bmatrix} \tag{15}$$

$$C_{invc}=\begin{bmatrix}\begin{bmatrix}T_{ci} & 0 & 0\end{bmatrix} & 0 & 0 & \begin{bmatrix}0 & 0 & T_{si}\end{bmatrix}\end{bmatrix} \tag{16}$$

$$B_x=\begin{bmatrix}T_v^{-1} & 0 & 0\end{bmatrix} \tag{17}$$

2.1.2. The Combined Model of All Inverters

The small-signal state-space model of the inverter in the common rotating coordinate system can be obtained via Equations (18) and (19).

 doi:10.20944/preprints202510.1718.v1

$$[\Delta \dot{x}_{invi}] = A_{invi}[\Delta x_{invi}] + B_{invi}[\Delta v_{gDQi}] + B_{1\omega com} C_{inv\omega i}[\Delta \omega_{com}] \quad (18)$$

$$[\Delta i_{oDQ}] = [C_{invci}][\Delta x_{invi}] \quad (19)$$

The rotational coordinate system selected for inverter 1 is regarded as the common rotational coordinate system. This enables the derivation of the state equations for the microgrid inverter network system, comprising all droop-controlled inverter units, as shown in Equation (20).

$$\begin{aligned} [\Delta \dot{X}_{INV}] &= A_{INV}[\Delta X_{INV}] + B_{INV}[\Delta v_{gDQ}] \\ [\Delta i_{oDQ}] &= [C_{INVc}][\Delta X_{INV}] \end{aligned} \quad (20)$$

where

$$[\Delta X_{INV}] = [\Delta x_{inv1} \quad \Delta x_{inv1} \quad \Delta x_{inv1}] \quad (21)$$

$$[\Delta i_{oDQ}] = [\Delta i_{oDQ1} \quad \Delta i_{oDQ2} \quad \Delta i_{oDQ3}] \quad (22)$$

$$A_{INV} = \begin{bmatrix} A_{inv1} + B_{1\omega com} C_{inv\omega 1} & 0 & 0 \\ B_{1\omega com} C_{inv\omega 1} & A_{inv2} & 0 \\ B_{1\omega com} C_{inv\omega 1} & 0 & A_{inv3} \end{bmatrix} \quad (23)$$

$$B_{INV} = \begin{bmatrix} B_{inv1} & 0 & 0 \\ 0 & B_{inv2} & 0 \\ 0 & 0 & B_{inv3} \end{bmatrix} \quad (24)$$

$$C_{INV} = \begin{bmatrix} C_{inv1} & 0 & 0 \\ 0 & C_{inv2} & 0 \\ 0 & 0 & C_{inv3} \end{bmatrix} \quad (25)$$

2.1.3. Network Bus Model

The small-signal model of the busbar line network at nodes i and i+1 in the system may be expressed as given in Equation (26).

$$\Delta \dot{i}_{lineDQi} = A_{NETi}[\Delta i_{lineDQi}] + B_{1NETi}[\Delta v_{gDQ}] + B_{2NETi}[\Delta \omega_{com}] \quad (26)$$

$$A_{NETi} = \begin{bmatrix} -\frac{R_{linei}}{L_{linei}} & \omega_0 \\ -\omega_0 & -\frac{R_{linei}}{L_{linei}} \end{bmatrix} \quad (27)$$

$$B_{2NETi} = \begin{bmatrix} l_{lineQi} \\ -l_{lineDi} \end{bmatrix} \quad (28)$$

$$B_{1NET} = \begin{bmatrix} B_{1NET1} \\ B_{1NET2} \\ B_{1NET3} \end{bmatrix}, B_{2NET} = \begin{bmatrix} B_{2NET1} \\ B_{2NET2} \\ B_{2NET3} \end{bmatrix} \quad (29)$$

 doi:10.20944/preprints202510.1718.v1

$$A_{NET}=\begin{bmatrix} A_{NET1} & 0 & 0 \\ 0 & A_{NET2} & 0 \\ 0 & 0 & A_{NET3} \end{bmatrix} \tag{30}$$

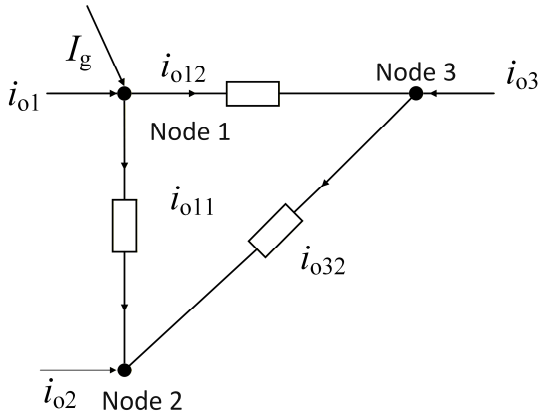

Figure 4. The network connection diagram of the closed-loop microgrid system.

2.1.4. Load Model

The RL load small signal model at the i th node of the system can be expressed in the following (31).

$$\Delta \dot{i}_{loadDQi}=A_{NETi}\left[\Delta i_{loadDQi}\right]+B_{1LOADi}\left[\Delta v_{gDQ}\right]+ B_{2LOADi}\left[\Delta \omega_{com}\right] \tag{31}$$

$$A_{LOADi}=\begin{bmatrix} -\frac{R_{loadi}}{L_{loadi}} & \omega_0 \\ -\omega_0 & -\frac{R_{loadi}}{L_{loadi}} \end{bmatrix} \tag{32}$$

$$B_{2LOADi}=\begin{bmatrix} l_{loadQi} \\ -l_{loadDi} \end{bmatrix} \tag{33}$$

$$B_{1LOAD}=\begin{bmatrix} B_{1load1} \\ B_{1load2} \\ B_{1load3} \end{bmatrix}, B_{2LOAD}=\begin{bmatrix} B_{2load1} \\ B_{2load2} \\ B_{2load3} \end{bmatrix} \tag{34}$$

$$A_{LOAD}=\begin{bmatrix} A_{LOAD1} & 0 & 0 \\ 0 & A_{LOAD2} & 0 \\ 0 & 0 & A_{LOAD3} \end{bmatrix} \tag{35}$$

2.1.5. A Complete Microgrid Model

The complete microgrid consists of multiple inverters, closed-loop circuit line loads, and local loads of each inverter. The state equation and its small-signal state model can be constructed by combining the models of each subsystem, so the small-signal model of the microgrid system in the common rotating coordinate system is obtained.

 doi:10.20944/preprints202510.1718.v1

$$\begin{bmatrix} \Delta\dot{X}_{INV} \\ \Delta\dot{i}_{lineDQ} \\ \Delta\dot{i}_{loadDQ} \end{bmatrix} = A_{MG} \begin{bmatrix} \Delta X_{INV} \\ \Delta i_{lineDQ} \\ \Delta i_{loadDQ} \end{bmatrix} + B_{MG} \begin{bmatrix} \Delta v_{gDQ} \end{bmatrix}$$
$$\begin{bmatrix} \Delta i_{oDQ} \end{bmatrix} = C_{MG} \begin{bmatrix} \Delta X_{INV} \\ \Delta i_{lineDQ} \\ \Delta i_{loadDQ} \end{bmatrix} \quad (36)$$

2.2. Stability Analysis

Eigenvalue analysis is a key means of studying the stability of linearised systems and essentially depends on the distribution characteristics of the system state matrix's eigenvalues in the complex plane. According to the theory of linear systems, the stability of a system can be strictly determined by the sign of the real part of an eigenvalue: if all the eigenvalues have negative real parts and lie the left-half plane, the system is asymptotically stable at the equilibrium point; conversely, if at least one of the eigenvalues has a positive real part, the system is unstable. When the real part of an eigenvalue is zero and its algebraic and geometric multiplicities are equal, the system is in a critical stable state. In practical applications, however, it is generally considered that the system is not robust. Furthermore, the absolute value of the real part of the eigenvalue reflects the attenuation rate of the corresponding mode, and the imaginary part determines the oscillation frequency. Notably, the dominant eigenvalue closest to the imaginary axis plays a pivotal role in the transient response performance of the system. Based on the fifty-one-dimensional microgrid system model that has been established, this paper provides a comprehensive analysis of the system's stability and dynamic characteristics by solving for all the eigenvalues according to the aforementioned distribution rules.

Sensitivity analysis utilizes sensitivity indices to evaluate system stability and is widely used in both conventional power systems and microgrids. In the context of eigenvalue analysis, the sensitivity of eigenvalues to variations in system parameters is examined to quantify their impact on state variables. This information, combined with eigenvalue data, facilitates the rational selection of key controller parameters, such as the power droop coefficient.

3. Results & Discussion

Based on the above analysis, the following simulation verification is conducted.

3.1. Stability Analysis

3.1.1. Eigenvalue Analysis

The eigenvalue analysis method, which extracts key stability indices—such as oscillation frequency, amplitude, and damping ratio—by solving the eigenvalues of the system state matrix, is widely employed in small-signal stability analysis of microgrids due to its conceptual clarity and rigorous criteria [26].

The dimension of the system model is determined by the three parts: the inverter section, the busbar line section, and the load section. In this paper, the microgrid composed of three parallel inverters is taken as the research object. The model dimension of a single inverter is 13, corresponding to thirteen state variables. Therefore, the dimension of the subsystem composed of the three inverters is 39. On this basis, the overall dimension of the system is fifty-one-dimensional, corresponding to 51 eigenvalues.

Inputting the data from Table 1 into the simulation system yields the operational data at the steady-state operating point, as shown in Table 2. The distribution of eigenvalues for the microgrid experimental system's state equations, computed using MATLAB, is illustrated in Figure 5. It can be

 doi:10.20944/preprints202510.1718.v1

observed that all eigenvalues lie within the left-half plane of the complex plane, indicating that the microgrid experimental system is stable [27].

Table 1. Main parameters of the closed-loop microgrid system.

Classification of Parameters	Parameter Symbol	Base Value
System Base Parameters	Rated Capacity, S（kVA）	50
	Rated Line-to-Line Voltage, V（V）	380
	Rated Frequency, f（Hz）	50
Inverter Unit	DC-Link Voltage, V_dc（V）	220
LC Filter	Inverter-Side Inductance, L1（H）	3e-3
	Filter Capacitance ,Cf（F）	20e-6
Droop Control	Active Power-Frequency Droop Coefficient,m（rad/W*s）	3.14e-4
	Reactive Power-Voltage Droop Coefficient,n（V/Var）	1e-3
Other parameters	Grid-Side Inductance,L2（H）	7e-3
	Line inductance,Lline(H)	3e-5
	Line resistance,Rline(Ω)	4e-5

Table 2. System stability parameter values.

Number of inverters (i = 1,2,3）	Steady-state operating point data
Steady-state angular frequency(ω_0/rad·s-1)	314.16214.9527
The phase difference relative to the common rotating coordinate system (**δ**i/rad)	（0，0.0066，-5.59e-8）
Output voltage in common rotating coordinate system (V_{gDi} , V_{gQi})/V	(214.95，-13.11) (214.89，-12.95) (-214.95，-13.11)
Inverter output voltage(V_{odi}, V_{oqi}) / V	(214.89,-12.95) (-214.95,-13.11) (214.89,-12.95)
Inverter output current (I_{odi}, I_{oqi}) / A	(214.89,-12.95) (-214.95,-13.11) (214.89,-12.95)
Inverter-side current (I_{fdi}, I_{fqi}) / A	(215.15,84.31) (214.99,84.49) (215.07,84.22)

 doi:10.20944/preprints202510.1718.v1

Inverter local load current (I_{loadDi}, I_{loadQi}) / A	(0.0772,-0.01) (0.0767,-0.01) (0.0767,-0.01)
Line current (I_{lineDi}, I_{lineQi}) / A	(215.35,0.032) (0,0) (215.35,0.032)

After adjusting the key parameters according to the pattern observed in Table 3, these settings were applied to the simulation system. New simulation results were obtained and incorporated into the mathematical model for computation, yielding the new eigenvalue distribution shown in Figure 6. The figure indicates that the system eigenvalues have shifted overall to the right, with some eigenvalues migrating into the right-half plane. According to eigenvalue analysis theory, this distribution confirms that the system has become unstable.

Table 3. System stability parameter values.

Parameters	Kpc	Kpv
Stable Condition	95	3
Unstable Condition	0.95	30

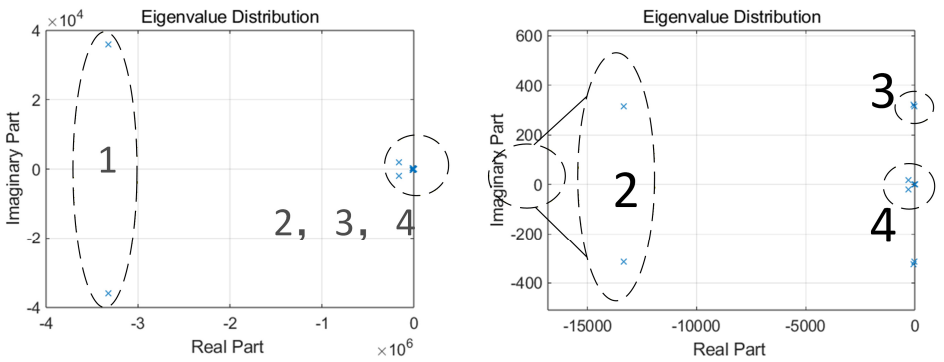

(a) (b)

Figure 5. Eigenvalue Distribution of the Microgrid State-Space Model under Steady-State Conditions. (a)Overall View of Eigenvalues;(b)Zoomed-in View of Local Eigenvalues.

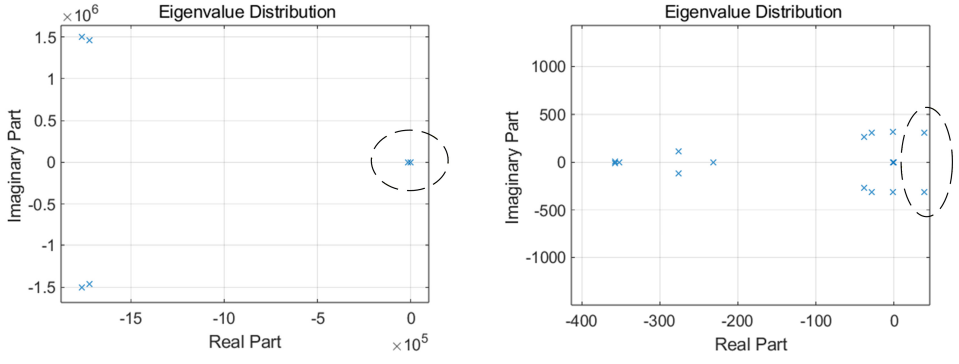

(a) (b)

Figure 6. Eigenvalue Distribution of the Microgrid State-Space Model under Unsteady-State Conditions. (a) Overall View of Eigenvalues;(b)Zoomed-in View of Local Eigenvalues.

 doi:10.20944/preprints202510.1718.v1

3.1.2. Sensitivity Analysis

Figure 5 shows the distribution of all 51 eigenvalues of the system under the initial conditions specified in Table 1. It can be observed that these eigenvalues exhibit a wide range of frequency components, which can be grouped into four distinct clusters.

The further the real part deviates from the imaginary axis, the faster the system's decay rate becomes, enabling quicker stabilization; conversely, the further the imaginary part deviates from the real axis, the higher the system's oscillation frequency becomes. As observed in Figure 5, the high-frequency mode labeled '1' corresponds to the state variables of the inverter's LC filter, exhibiting substantial real and imaginary components. During stable system operation, this mode exerts limited influence on overall stability. However, improper parameter design may induce high-frequency oscillations or resonances, thereby indirectly jeopardizing the system's stable functioning. As can be seen from Figure 5, dual voltage-current control determines the stability at medium and high frequencies. Unlike droop control, it does not directly render the system unstable, but rather determines the magnitude of the system's stability margin. It plays a crucial role in the local stability of the system, such as in the case of droop control numbers '2' and '3'.Droop control governs low-frequency oscillations. An improperly set droop coefficient causes the dominant system eigenvalue to approach the imaginary axis or even enter the right-half plane, thereby triggering low-frequency oscillations or voltage instability. Consequently, droop control represents the most sensitive element in system stability. As indicated by number '4', this mode lies closest to both the imaginary and real axes, rendering it most sensitive to parameter variations.

The distribution of parameter variations shown in Figure 7 indicates that changes in the LC filter parameters (Lf, Cf) and grid-side inductance Lg exert the most significant influence on system stability, potentially causing the system to transition from a stable to an unstable state. These parameters also exert a substantial effect on the oscillation frequency, and droop controller parameters play a pivotal role in system stability. The findings in Figure 7 further validate theoretical analysis: compared to power droop gain, the voltage and current loops primarily influence high-frequency characteristics within the system, while LC filter parameters predominantly affect low-frequency gain. Assessing eigenvalue displacement within identical parameter variation ranges reveals that the droop controller exhibits the highest sensitivity, followed by the LC filter.

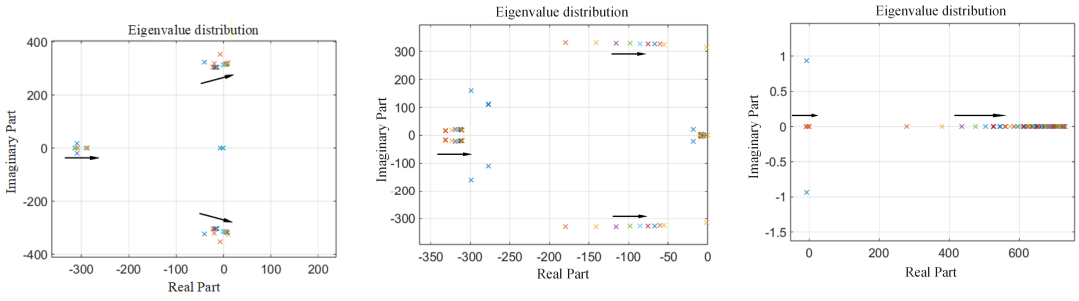

(a) (b) (c)

Figure 7. Changes of eigenvalues with LC parameters, voltage, and current loop coefficient and droop coefficient. (a)Changes of eigenvalues with LC parameters;(b)Changes of eigenvalues with voltage and current loop coefficient;(c)Changes of eigenvalues with droop coefficient.

3.1.3. Verification of the Model

Figure 8 consolidates the Simulink simulation results obtained using the parameter sets specified in Tables 2 and 3. Subplots (a), (b), and (c) correspond to the simulation case employing the parameters from Table 2, whereas Subplots (d), (e), and (f) present the results for the parameter set from Table 3.

 doi:10.20944/preprints202510.1718.v1

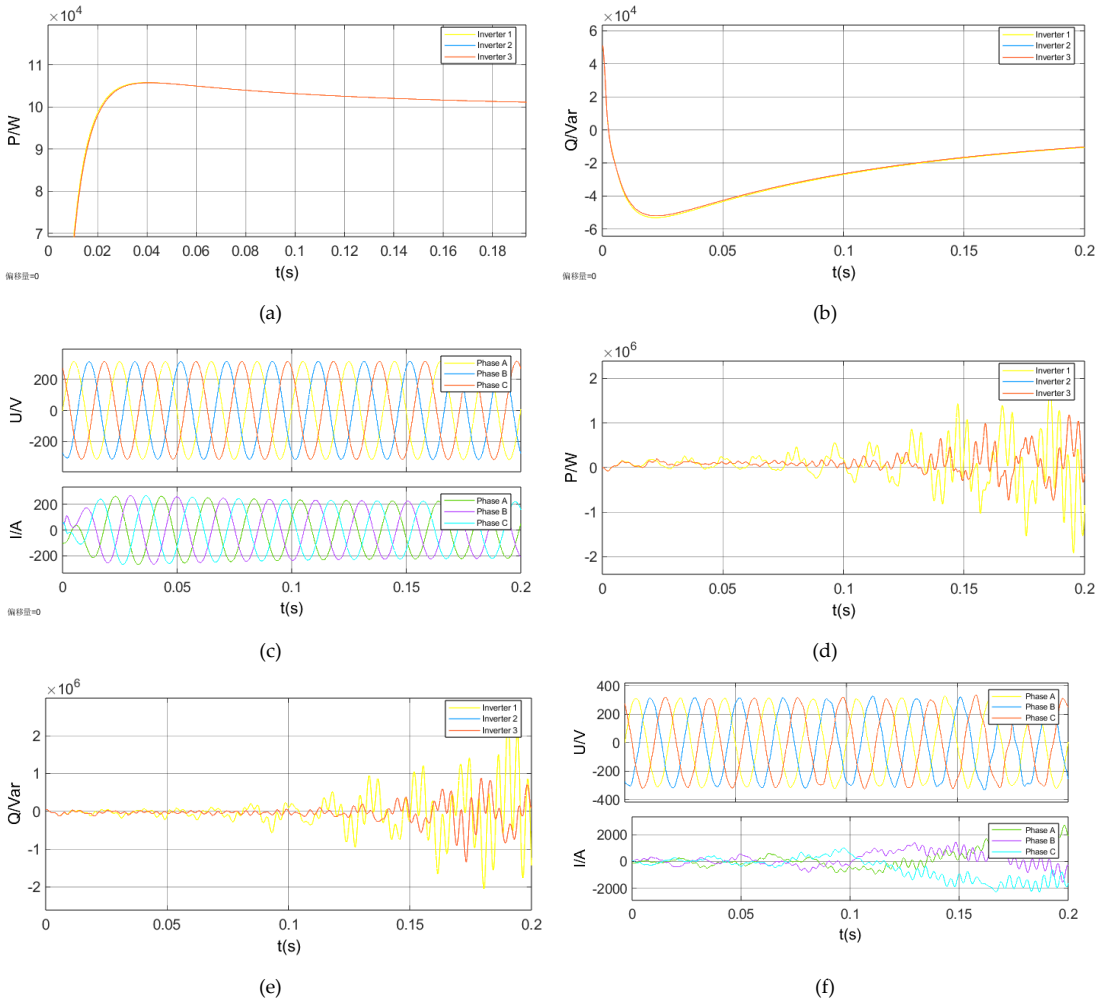

Figure 8. Simulated Waveforms of Output Active Power, Reactive Power, Voltage, and Current Under Stable and Unstable Conditions. (a)Waveform of Output Active Power under Stable Conditions;(b)Waveform of Output Reactive Power under Stable Conditions;(c)Waveforms of Output Voltage and Current under Stable Conditions;(d)Waveform of Output Active Power under Unstable Conditions;(e)Waveform of Output Reactive Power under Unstable Conditions;(f)Waveforms of Output Voltage and Current under Unstable Conditions.

From the simulation results shown in Figure 8, it can be seen that the output voltage, current, active power, and reactive power of the system remain stable. Furthermore, the active and reactive power output curves of the three inverters are nearly identical, indicating accurate power sharing. These results demonstrate the high stability of the system under parallel operation, which not only enhances the reliability of the microgrid but also helps prevent equipment overload caused by unbalanced power distribution, thereby extending the service life of the components.

However, simulation results from Figure 8 indicate that the system's output voltage, current, active power, and reactive power all exhibit oscillations and have become unstable. This behavioral discrepancy aligns perfectly with the predictions of the eigenvalue analysis. The high consistency between the Simulink simulation results and the predictions of the state-space model—where stable waveforms occur exclusively under theoretically stable conditions—provides strong validation for the accuracy and effectiveness of the theoretical modeling framework.

Thus, the established state-space model enables a rapid and precise assessment of system stability.

 doi:10.20944/preprints202510.1718.v1

3.2. Time-Domain Stability Analysis

3.2.1. Case 1: A 5% Step Increase in the Active Power Command in Droop Control

In grid-connected mode, a step disturbance signal with an amplitude of 5% of the rated active power is applied at t=0.5s. The system dynamic response simulation results are shown in Figure 9. The specific analysis is as follows:

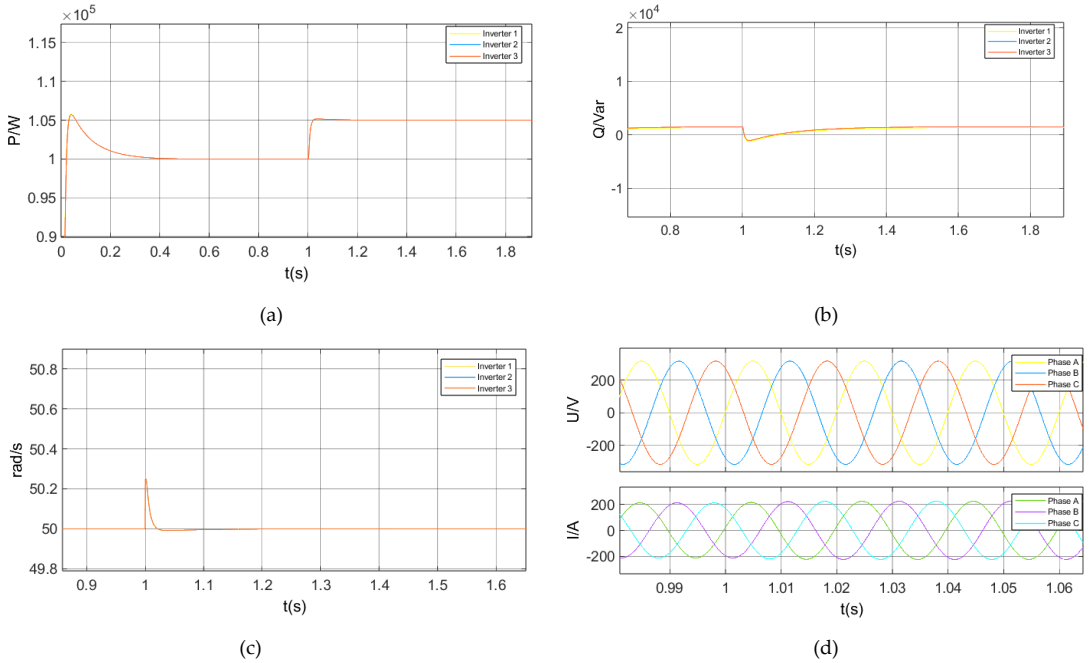

Figure 9. System Response to a 5% Increase in Active Power Command. (a) Waveform of Output Active Power;(b) Waveform of Output Reactive Power;(c) Waveform of Output Frequency;(d) Waveforms of Output Voltage and Current.

At t=0.5s, the active power suddenly increases by 5%. This occurs because the command value P0 undergoes a step increase, while the inverter's current output power P has not yet responded in time, resulting in a power difference. This difference serves as additional input to the droop controller, causing an increase in the inverter's output power.

Reactive power remains unchanged. The inverter's reactive power output primarily depends on the reactive power command value and is independent of active power; hence, the output remains constant. A slight dip occurs during the transient process, but eventually stabilizes and recovers to its initial value with grid support.

A brief frequency step occurs. According to the active-frequency droop relationship, power changes cause frequency fluctuations. During dynamic regulation, the inverter's internal PLL and dual-loop controller slightly increase the phase and frequency of the output voltage, resulting in a temporary rise. Due to the strong frequency support provided by the utility grid in grid-connected mode, the inverter's frequency resynchronizes with the grid frequency during steady state, ultimately returning to the initial value.

The output voltage remains unchanged. According to the reactive power-voltage control relationship, its steady-state value matches the initial value.

The output current remains unchanged. Under conditions of constant voltage, a 5% increase in active power, and unchanged reactive power, the current magnitude increases accordingly based on the apparent power relationship.3.2.2 Case 2: A 5% Step Decrease in the Reactive Power Command in Droop Control

 doi:10.20944/preprints202510.1718.v1

In grid-connected mode, a step disturbance with an amplitude of −5% of the rated reactive power is applied at t = 0.5 s. The system dynamic response simulation results are shown in Figure 10, with the following specific analysis:

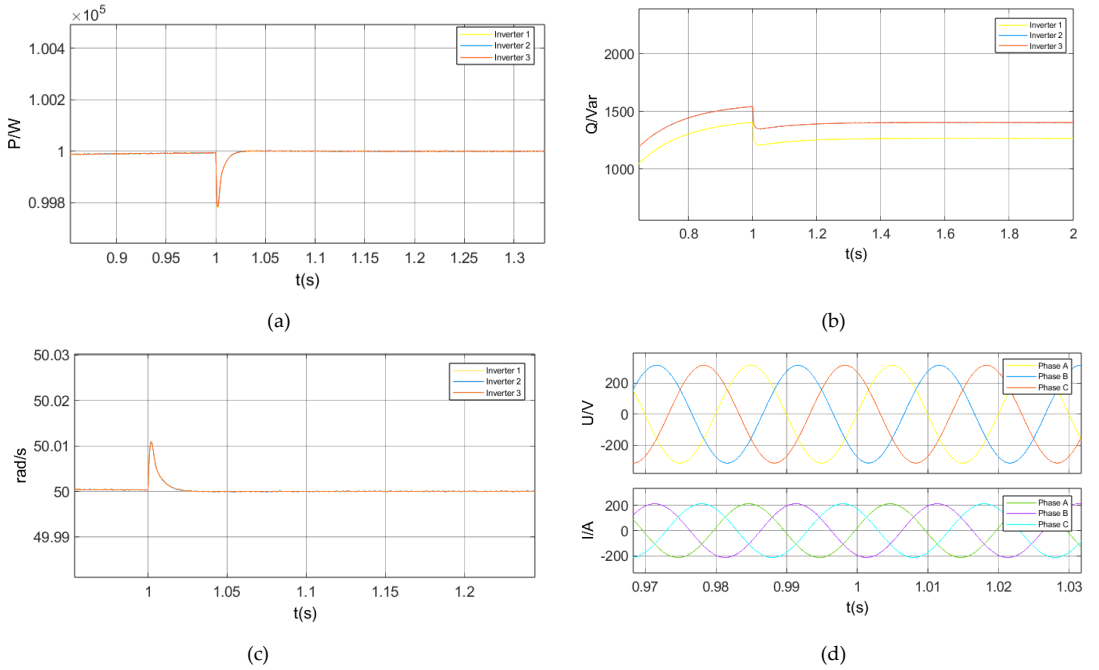

Figure 10. System Response to a 5% Decrease in Reactive Power Command. (a) Waveform of Output Active Power;(b) Waveform of Output Reactive Power;(c) Waveform of Output Frequency;(d) Waveforms of Output Voltage and Current.

Reactive Power: A sudden drop of approximately 5% occurs at t = 0.5 s. This results from the step decrease in the reactive power setpoint Q_0, while the actual reactive power output Q from the inverter has not yet responded in time, causing an instantaneous power deviation. This deviation is fed into the control system, driving the inverter to reduce its reactive power output.

Active Power and Frequency: Within the range of small steady-state disturbances, the P–f loop and Q–V loop can be considered decoupled. Therefore, altering reactive power has essentially no effect on active power. Simultaneously, the grid frequency is clamped at its rated value. According to the active power–frequency control relationship, the frequency remains largely constant during the disturbance, and any transient fluctuations that occur are negligible.

Output Voltage: Based on the reactive-voltage control relationship, the inverter control attempts to reduce the output voltage magnitude. However, in grid-connected mode, the grid provides strong voltage support, effectively locking the common grid point voltage at the grid level. Consequently, the output voltage remains generally stable.

Output Current: With voltage remaining essentially unchanged, reactive power reduced by 5%, and active power unchanged, the current magnitude should correspondingly decrease based on the apparent power relationship. The waveform trend in the figure aligns with this expectation. Although the reduction is not very pronounced, the current is observed to decrease by approximately 1–2 A using the vernier measurement tool.

3.2.3. Case 3: A 5% Step Increase in the Active Power Load at the PCC in Droop Control

In grid-connected mode, when a step disturbance with an amplitude of 5% of the power load is applied at the PCC point at t=0.6s, the system dynamic response simulation results are shown in Figure 11. The specific analysis is as follows:

 doi:10.20944/preprints202510.1718.v1

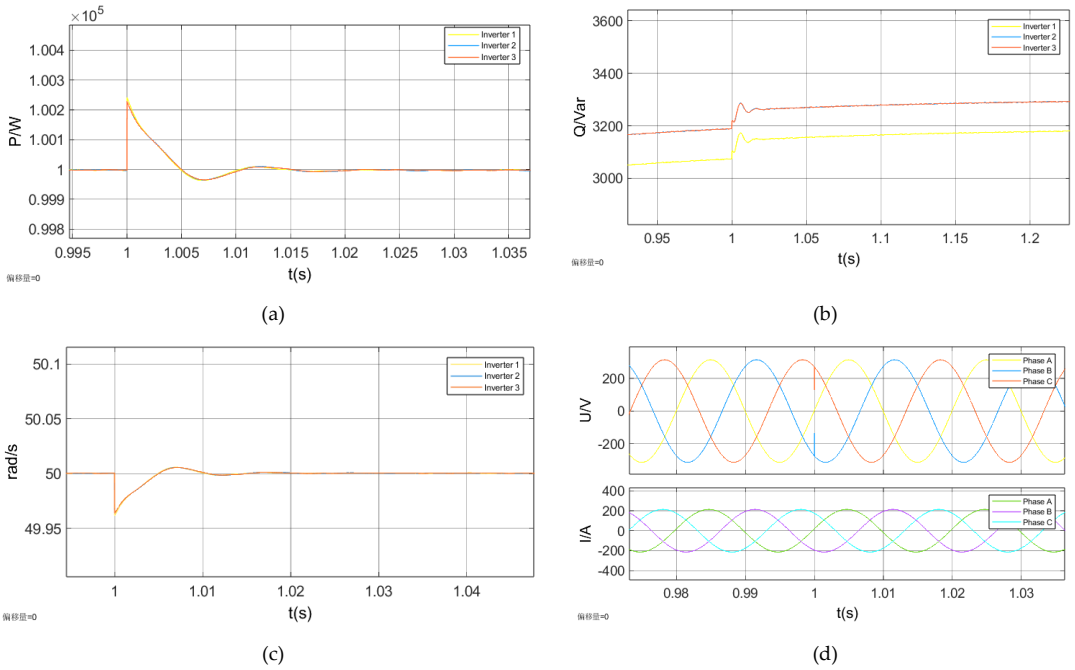

Figure 11. System Response to a 5% Step Increase in Power Load. (a) Waveform of Output Active Power;(b) Waveform of Output Reactive Power;(c) Waveform of Output Frequency;(d) Waveforms of Output Voltage and Current.

At t=0.6s, the active load at the PCC point suddenly increases by 5%. To meet this sudden power demand, the system utilizes its inertia, causing an extremely small and rapid drop in system frequency. The local inverter, based on the P-f droop relationship, counteracts this frequency decline by increasing active power output. This mitigates the depth and speed of the frequency drop, preventing false tripping of protection devices. Simultaneously, the large grid, leveraging its substantial inertia and robust speed regulation system, begins injecting additional active power into the PCC point. This forcefully pulls the system frequency back to and maintains it at the rated value. Concurrently, the active power stabilizes at a level higher than the initial value. Using the cursor measurement tool reveals that this increase is primarily due to the large grid assuming the additional active load.

Similar to active power, the reactive power curve exhibits an upward step at t=1s, subsequently stabilizing at a higher level, indicating the system's increased demand for reactive power. The Q-V droop control loop automatically boosts reactive output to support voltage, while the large grid also provides voltage support. The failure of reactive power to return to its initial value indicates that the three inverters collectively bear the new reactive load.

The voltage experiences an extremely slight dip before rsapidly recovering and stabilizing. Based on the relationship between power and voltage/current, an increase in active power corresponds to a corresponding increase in current, as shown in Figure 11.

The simulation results in Figures 9–11 reveal the system's dynamic response to minor disturbances: all observed variables converge to new stable values after transient oscillations. Notably, these stable values are jointly determined by the system's operating mode and the specific components affected by the disturbance. In summary, the system demonstrates the capability to maintain stable operation following minor disturbances.

4. Conclusions

This paper presents a systematic investigation into the stability of closed-loop microgrids, spanning theoretical modeling to simulation verification. By establishing an accurate state-space

 doi:10.20944/preprints202510.1718.v1

model supplemented with eigenvalue analysis and parameter sensitivity analysis, it thoroughly reveals the key modes and dominant factors influencing system stability. The research confirms that droop control coefficients and LC filter parameters exert the most significant influence on system dynamics, providing clear theoretical foundations and design guidance for optimizing microgrid controller parameters.

To validate the mathematical model's effectiveness, time-domain simulation analysis was further conducted. Results demonstrated perfect alignment between the stability boundaries predicted by eigenvalue analysis and the system's time-domain dynamic response, conclusively proving the state-space model's capability to accurately capture the stability boundaries of the closed-loop microgrid model. Finally, multiple simulation experiments were conducted to investigate the dynamic characteristics of the closed-loop structured microgrid under grid-connected operation. These experiments demonstrated that the time-domain approach enables clear observation of system dynamics. Additionally, stability analysis was performed under grid-connected conditions after introducing small disturbances to rated power and load power components, confirming that minor disturbances do not compromise system stability in this mode.

The modeling and analysis methodology established in this study, along with the investigation of closed-loop microgrid structures, provides effective tools and novel insights for stability analysis and optimization design of complex microgrid systems. This research holds significant theoretical guidance for advancing microgrid technology development and engineering applications. Future studies may further explore critical issues such as system characteristics in islanded mode and the performance of hybrid control modes incorporating synchronous controllers.

References

1. S. A. Arefifar; M. Ordonez; Y. Mohamed. Energy management in multi-microgrid systems — development and assessment. 2017 IEEE Power & Energy Society General Meeting, Chicago, IL, USA, 2017, 1-1.
2. Farzin Hossein; M. Fotuhi-Firuzabad; M. Moeini-Aghtaie. Enhancing Power System Resilience Through Hierarchical Outage Management in Multi-Microgrids. IEEE Trans. Smart Grid. 2016,7,2869-2879.
3. T. Meng; Z. Lin; Y. Wan; Y. A. Shamash. An Output Regulation Approach to Distributed Voltage Regulation of Multiple Coupled Distributed Generation Units in DC Microgrids, in 2022 American Control Conference (ACC), Atlanta, GA, USA, 2022, 4534-4539.
4. Dong Zhaoyang; Zhao Junhua; Wen Fushuan; XUE Yusheng. From smart grid to energy Internet: Basic concept and research framework. AEPS,2014,38,15,1-11.
5. Ma Zhao; Zhou Xiaoxin; Shang Yuwei; SHENG Wanxing. Exploring the Concept, Key Technologies, and Development Model of Energy Internet. PST,2015,39,113014-3022.
6. J. de la Cruz; Y. Wu; J. E. Candelo-Becerra; J. C. Vásquez; J. M. Guerrero. Review of Networked Microgrid Protection: Architectures, Challenges, Solutions, and Future Trends. CSEEJ POWER ENERGY, March 2024,10, 448-467.
7. Sui X, Tang Y, He H; Wen, J.Energy-Storage-Based Low-Frequency Oscillation Damping Control Using Particle Swarm Optimization and Heuristic Dynamic Programming. IEEE Trans. Power Syst, 2014,29,2539-2548.
8. Z Zeng; R ZHAO; Lü Z; L Ma. Impedance Reshaping of Grid-tied Inverters to Damp the Series and Parallel Harmonic Resonances of Photovoltaic Systems. In Proceedings of the CSEE. 2014, 34, 45747-4558.
9. LI Junjie; LÜ Zhenyu; WU Zaijun; LIU Haijun; YANG Shihui. Adaptive switching strategy of AC/DC hybrid microgrid operating mode based on the power electronic transformer. Electric Power Automation Equipment, 2020,40,126-131+138.
10. SUN Zhenao; YANG Zilong; WANG Yibo; XU Hongbo. A Hybrid Islanding Detection Method for Distributed Multi-inverter Systems. In Proceedings of the CSEE. 2016,36,3590-3597+3378.
11. GU Xiaofeng; YUAN Xufeng; ZHENG Huajun; XIONG Wei. Review of AC/DC hybrid microgrid stability analysis and its enhancement measures. Distribution & Utilization. 2025,42,8-20.
12. Guerrero, Josep M. et al. Advanced Control Architectures for Intelligent Microgrids—Part I: Decentralized and Hierarchical Control. IEEE Trans. Ind. Electron, 2013,60,1254-1262.

 doi:10.20944/preprints202510.1718.v1

13. Xu, Yuqin; Fang, Nan. Control strategy research and simulation analysis of an independent optical storage microgrid based on voltage stabilizing control. Power System Protection and Control. November 1, 2020,48, 67-74.
14. Feng Wei; Sun Kai; Guan Yajuan; Josep M.Guerrero; XIAO Xi. An Active Harmonic Grid-Connecting Current Suppression Strategy for Hierarchical Control-Based Microgrid. Transactions of China Electrotechnical Society, March 25, 2018,33, 1400-1409.
15. M. Li, X. Zhang, X. Fu, H. Geng, and W. Zhao. Stability Studies on PV Grid-connected Inverters under Weak Grid: A Review. Chinese Journal of Electrical Engineering, December 2024,10, 1-19.
16. Lopes, J. A. Pecas; C. L. Moreira; A. G. Madureira. Defining control strategies for Micro Grids islanded operation. IEEE Trans. Power Syst. 2006,21,916-924.
17. Liu Xu; Zhang Guoju; Pei Wei; ZHU Enze; ZHANG Xue. Current status and development trends of grid-type converters. Acta Energiae Solaris Sinica 2024,45,101-111.
18. HUANG Xianmiao1; SHAO Yichi; GONG Yu; LIU Di; ZHU Xuesen; LUO Jiasen. Control technology for grid-forming energy storage under unbalanced working conditions of weak current networks. Thermal Power Generation,2024, 53, 59-67.
19. WU Yuanyao; XIAO Shiwu. Static Voltage Stability Analysis of New Energy Islanded Microgrids Supported by Grid-forming Energy Storage. PST,2025,1-14.
20. M. Lu, Y. Yang; B. Johnson; and F. Blaabjerg. An Interaction-Admittance Model for Multi-Inverter Grid-Connected Systems. TPE, Aug. 2019, 34, 7542-7557.
21. N. Pogaku; M. Prodanovic; T. C. Green. Modeling, Analysis, and Testing of Autonomous Operation of an Inverter-Based Microgrid.TPE, March 2007,22, 613-625.
22. He Jinwei; Yun Wei Li. An Enhanced Microgrid Load Demand Sharing Strategy. TPE, 2012, 27,3984-3995.
23. SHI Jie; ZHENG Zhanghua; AI Qian. Modeling of DC micro-grid and stability analysis. Electric Power Automation Equipment,2010, 30, 86-90.
24. Wang Shuya; Su Jianhui; Yang Xiangzhen; DU Yan. A review of the small signal stability of the microgrid. Electr. Eng, 2016,11,39-45.
25. LIU Hong; BAO Mingyang; LU Shaohan; DUAN Qing; SHENTU Leixuan; HUANG Yuanping. Coordinated operation method of the distribution network and multiple microgrids considering network reconfiguration. Electric Power Automation Equipment, 2025,45, 114-121,
26. Xiang Yang; Fu Ming; Zhang Aifang; DOU Xiaobo; JIAO Yang; YANG Yeqing. Small signal stability analysis of AC/DC hybrid microgrid under isolated island operation. Electric Power Construction, 2017,38,96-105.
27. Zheng Jinghong; Li Xingwang; Wang Yanting; ZHU Shouzhen; WANG Xiaoyu; ZHU Hongbo. Small-signal stability analysis of a microgrid switching to islanded mode. Automation of Electric Power Systems, 2012,36,25-32.